A Time-Varying Log-linear Model for Predicting the Resistance of Lithium-ion Batteries

Vilsen, Søren Byg; Sui, Xin; Stroe, Daniel-Ioan

Published in:
IPEMC 2020-ECCE Asia

Publication date:
2020

Document Version
Accepted author manuscript, peer reviewed version

A Time-Varying Log-linear Model for Predicting the Resistance of Lithium-ion Batteries

Søren B. Vilsen
Department of Mathematical Sciences
Aalborg University
Aalborg, Denmark
svilsen@math.aau.dk

Xin Sui
Department of Energy Technology
Aalborg University
Aalborg, Denmark
xin@et.aau.dk

Daniel-Ioan Stroe
Department of Energy Technology
Aalborg University
Aalborg, Denmark
dis@et.aau.dk

***Abstract*—The resistance offers insight into the efficiency and power capability of Lithium-ion (Li-ion) batteries. That is, it can describe the performance of the batteries. However, as with other performance parameters of Li-ion batteries, the resistance is dependent on the operating conditions and the age of the battery. Traditionally, to capture these dependencies, Li-ion cells are aged at different conditions by applying synthetic mission profiles, which are periodically stopped to measure the resistance at standard conditions. Even though accurate information about the resistance behaviour are obtained, the measurements are time-consuming. Therefore, we extract the resistance directly from a dynamic real-life profile. The extracted resistance is modelled as function of the state-of-charge (SOC). The parameters of the model are allowed to vary over time to account for increase in the resistance as the battery ages. In order to capture the variation in time of the parameters of the log-linear model are assumed to follow a vector auto-regressive (VAR) model. The estimated VAR is used to predict the long term behaviour of the expected internal resistance. The prediction of the long term behaviour will enable the calculation of the remaining useful life of the battery, allowing for the inclusion of future battery usage through the SOC.**

***Index Terms*—Lithium-ion battery, Resistance estimation, Remaining useful lifetime prediction, Dynamic aging profile, Time-varying log-linear model**

I. Introduction

The resistance, together with the capacity, are the two parameters describing the performance and lifetime behaviour of a Lithium-ion battery [1]. The resistance is used to determine the batteries' power capability [2], important in both renewable energy storage and electric vehicle (EV) applications. Thus, it follows that in order to optimise the size requirements of a battery system, in both a technical and economical sense, having accurate knowledge of the resistance, and, therefore, the power capability is important.

The resistance of Li-ion batteries is a nonlinear parameter, which is changing depending on the operating temperature, load current, and on the battery state-of-charge (SOC) [3], [4]. Furthermore, the resistance of the battery increases with long-term operation resulting in a decrease of the battery power capability [5]. Even though different methods for determining the resistance of the Li-ion batteries exist [6], [7], it is usually measured by the current pulse technique: a charging/discharging current of a certain amplitude and length is applied to the battery and the voltage response of the battery is registered [2], [5]. After which, the resistance is calculated using Ohm's Law. This method is successfully applied in laboratory conditions. However, prior to the resistance measurement, the battery needs to be in idling mode to reach thermo-dynamic stability. This requirement makes the current-pulse method less suitable for real-life applications, where downtime of the Li-ion storage system is technical and/or economic infeasible. Nevertheless, previous work has shown that extraction of the resistance from a dynamic real-life profiles is feasible, and that the extracted resistance can be modelled as a function of SOC and aging [25].

If reference measurements can be performed during the ageing of the battery, then estimating the effect of ageing on the internal resistance is fairly simple. However, when the internal resistance is identified in a dynamic profile, modelling the degradation of the power becomes as lot more difficult. Modelling of the internal resistance can be broken into two categories: online and offline methods. Offline methods include: support vector machines (SVM), relevance vector machines (RVM), genetic algorithms (GA), particle swarm optimisation (PSO), artificial neural networks (ANN, or DNN if the network architecture contains many hidden layers), and appropriate combination of these methods [9]–[15]. The offline methods can predict both short and long term degradation behaviour with very high accuracy, but requires a large amount of information captured during the entire ageing period of the battery in order to achieve the requried accuracy. The most common online estimation method is by dual estimation of an equivalent electrical circuit (EEC) based state-space model, and capacity and resistance using a non-linear Kalman-filter variant (i.e. either an extended, or unscented Kalman-filter) [16]–[18], or in some instances the more general particle filters [19], [20]. This approach can be further improved by basing the state-space model on an Electrochemical model (EM), however, this comes with added computational complexity [21], [22]. Not all online methods are EEC or EM methods a notable exception is the series resistance determination (SRD) algorithm (also called the direct resistance estimation) [23]–[25]. While the online methods can be excellent at predicting the current state of the system, and the immediate future of the battery, predictions of the long term behaviour of the

degradation can be inaccurate.

The most prevalent reason for the inaccuracy of the online methods, is the highly volatile nature of the battery states, and the fast frequency used for updating what are slowly changing degradation parameters. To overcome this fault, a method is proposed to model the long term behaviour of the degradation. Assuming the resistance is extracted using the SRD based method proposed in [25], the parameters of the internal resistance model will be assumed to follow a vector auto-regressive (VAR) process [26]. The VAR will capture the long term time-varying behaviour of the parameters of the internal resistance model. Furthermore, by predicting the VAR model forward in time, it is possible to predict the remaining useful life (RUL) of the battery, by using Bayes' rule [27], the law of total probability [27], making assumptions about the prior probability of the SOC and week values.

II. Experiment

A. Lithium-ion battery under test

For this work we have used a high-power LiFePO4-based Li-ion battery with a capacity of 2.5 Ah and nominal voltage of 3.3 V.

B. Aging condition and internal resistance measurement

The battery was aged using the dynamic current profile presented in Fig. 1, which has a length of one week. When applied to the tested battery, the current profile resulted into the SOC profile, presented in Fig. 2, which varies in the interval 10% - 90% SOC. The aging profile presented in Fig. 1, was applied for a period of 38 weeks considering an aging temperature of 25^{o}C. For more details about the aging profile, the reader is referred to [28].

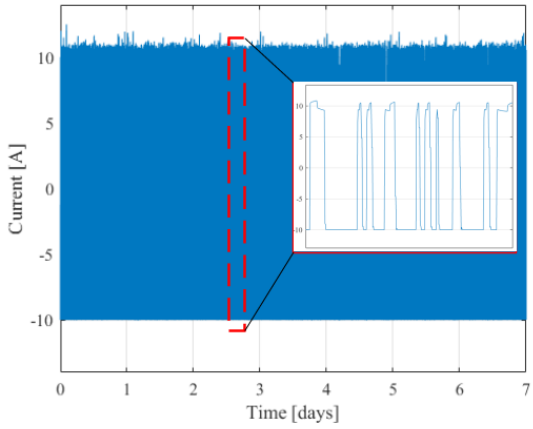

Fig. 1. One-week current profile used for aging the LFP-based Li-ion battery

After each week of aging tests, the resistance of the battery was determined using the current pulse technique; the measurements were carried out at 20%, 50% and 80% SOC, using a current pulse of 4C-rate (i.e., 10 A), which was applied for 18 seconds. Before the measurement, the battery was in idling mode for 15 minutes, in order to reach thermo-dynamic

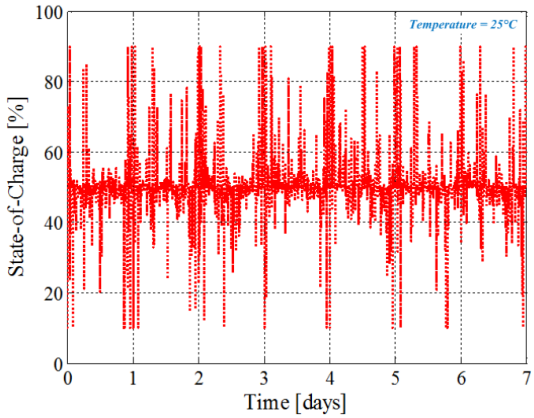

Fig. 2. The battery cell's SOC profile corresponding to one week of aging.

stability. The increase of the battery resistance during the 38 weeks of cycling is presented in Fig. 3. As one can observe, for the considered aging period, the resistance has increased only by 8.7%, even though the battery cell's capacity decreased by more than 15% in comparison to the value measured at the beginning of life, as it is presented in Fig. 4.

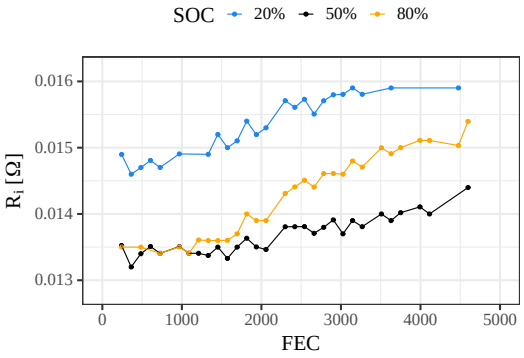

Fig. 3. The internal resistance increase during the aging test.

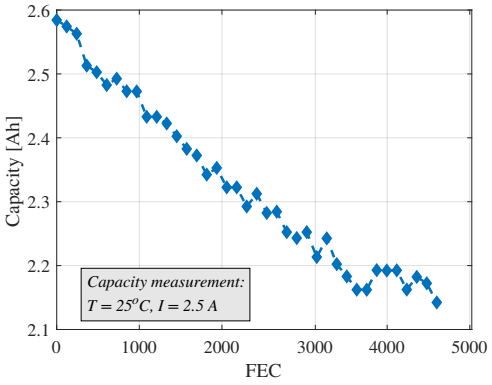

Fig. 4. The capacity fade behavior of the battery cell during the aging test.

III. Methodology

The battery resistance is extracted from the dynamic profile, presented in Fig. 1, by utilising the method presented in [25]. The method requires keeping very careful track of the following:

(1) Changes to the current: ΔI.
(2) The value of the voltage at the end of the last relaxation period V_s.
(3) Amount of time the battery was relaxed ΔT_{relax}.
(4) The length of the previous pulse $\Delta T_{previous}$.
(5) The length of the current pulse $\Delta T_{current}$.

Using these five variables, the internal resistance was extracted as the resistance value 18s after the beginning of the current pulse. Requiring a relaxation period at least as long as the previous pulse. That is, if $\Delta T_{relax} \geq \Delta T_{previous}$, then the resistance is calculated as:

$$R_i = \frac{V_{18s} - V_s}{\Delta I}. \tag{1}$$

A sketch illustrating the five items, and the extracted resistance is shown in Fig. 5.

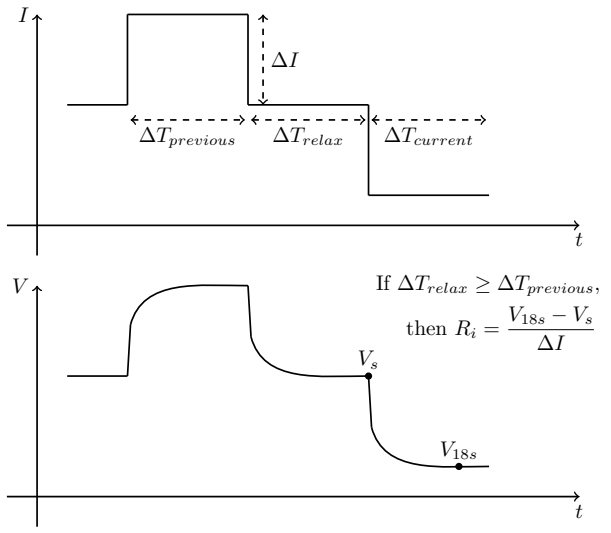

Fig. 5. Sketch of the resistance extraction method.

IV. Results

A. Internal resistance variation with SOC

Disregarding the effects of current (i.e., C-rate) and temperature, the resistance of the battery cell, only varies with the SOC. Based on previous studies [25], it has been shown that the battery resistance for a given week w can be modelled as:

$$R_i(\text{SOC}) = a_w \cdot \text{SOC}^{b_w} \cdot (1 - \text{SOC})^c, \tag{2}$$

which on a logarithmic scale becomes:

$$\begin{aligned} \log(R_i) = \beta_{0,w} + \beta_{1,w} \cdot \log(\text{SOC}) \\ + \beta_{2,w} \cdot \log(1 - \text{SOC}) + \varepsilon, \end{aligned} \tag{3}$$

where ε follows a normal distribution with mean zero variance σ_w^2. Considering the logarithm of Eq. (2), the relationship becomes linear in the parameter space, which is highly desirable for parameter estimation. The parameters in Eq. (3) are estimated by maximum likelihood [27] under the assumption that $\beta_{1,w}$ and $\beta_{2,w}$ are both smaller than, or equal to, 0. Furthermore, the parameters $\beta_{1,w}$ and $\beta_{2,w}$ control the curvature of the left and right side of the function, respectively. As a parameter decreases, the curvature of the corresponding side increases, and vice versa when a parameter tend towards zero, until the function is entirely flat on the corresponding side. While the three β parameters in combination control the lowest point of the function (found at SOC $= 0.5$). Note that this assumes that the SOC can never actually reach either 0 or 1 (in both cases Eq. (3) is undefined – in fact it is $-\infty$ in both cases).

An example of the model in Eq. (3) fitted to a week of extracted battery resistance is shown in Fig. 6. The continuous blue line, seen in the figure, is the expected logarithmic resistance of the model in Eq. (3) transformed back to the model in Eq. (2) by taking the exponential. The particular equation of the internal resistance (i.e. the continuous blue line) from week 16 is:

$$\hat{R}_i = 0.007 \cdot \text{SOC}^{-0.3921} \cdot (1 - \text{SOC})^{-0.3902}. \tag{4}$$

Fig. 6 shows that the model presented in Eq. (2) yields the expected parabolic relationship between the SOC and the internal resistance [29].

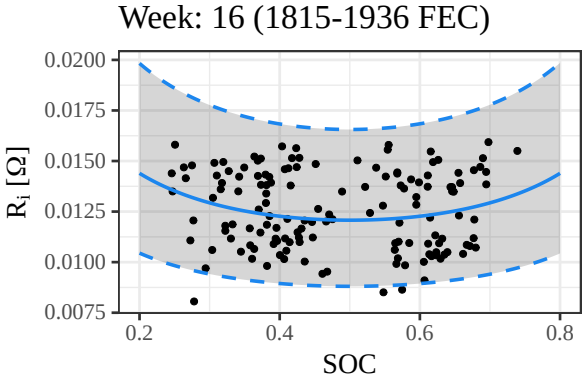

Fig. 6. The resistance against the SOC of week 16 (≈ 1815-1936 FEC). The extracted internal resistances are shown as black. Furthermore, the solid blue line corresponds to the expected mean of the resistance model in Eq. (3) fitted to the black points. While the blue dashed lines corresponds to a 95% prediction interval for the expected internal resistance of the model (solid blue line).

The evolution of the four parameters of the internal re-

sistance model (IRM), described in Eq. (3), can be seen in Fig. 7, showing the estimated parameters for every week in the ageing data. The figure shows that the evolution of the three mean parameters is nearly identical, though the scales are different. Furthermore, it shows that the variation seems to slowly increase over time. If it can be assumed the four parameters of the IRM encapsulate the expected and variational behaviour of the internal resistance on a week-by-week basis, then modelling the IRM parameters as a function of time would allow for the prediction of the internal resistance over time and, thereby, the degradation of the battery cell.

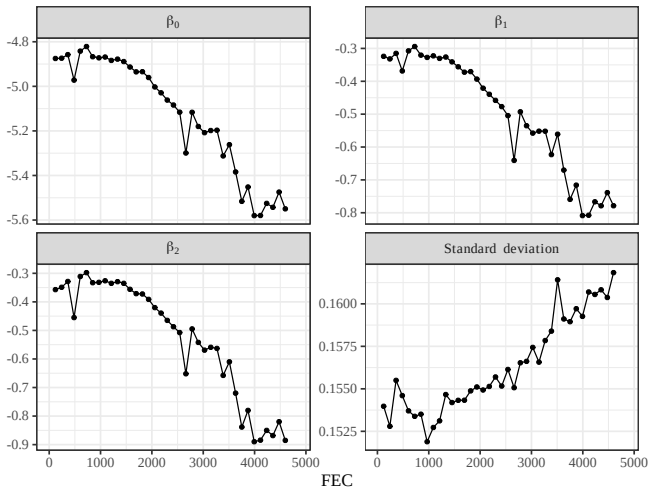

Fig. 7. The estimated parameters of the internal resistance model for every week.

B. Modelling battery resistance degradation

In order to predict the battery resistance degradation, two things are needed: (1) a model of the parameters as a function of time (in this case time is measured in weeks), and (2) additional information of SOC (as the IRM is highly dependent on the SOC).

1) Vector autoregressive process:

The three parameters describing the expected behaviour of the IRM, are highly dependent, as described above, and, therefore, the approach to modelling the change in these parameters, has to be both multivariate and time dependent. This implies that a vector autoregressive process, VAR, is necessary to capture the behaviour. In a VAR, the parameters of a week, w, depends on the past, i.e. $w-1$, $w-2$, ..., $w-l$. The subscript l is called the lag of the autoregression [26]. For this model to be applicable, the first l weeks are assumed to be known. A preliminary study showed that $l = 1$ is an appropriate lag, when modelling the parameters of the IRM.

Assuming that the parameters of the first week are known, then the vector of parameters of week w, denoted $\boldsymbol{\theta}_w = (\beta_{0,w}, \beta_{1,w}, \beta_{2,w}, \sigma_w)^T$, can be modelled as:

$$\boldsymbol{\theta}_w = c + \Gamma\boldsymbol{\theta}_{w-1} + \boldsymbol{\nu}_w, \tag{5}$$

where c, is a 4×1 vector of (intercept) coefficients, Γ is 4×4 matrix of time-invariant parameter coefficients, and $\boldsymbol{\nu}_w$ is a 4×1 white noise vector process. That is, $\boldsymbol{\nu}_w$ has to satisfy the following:

- $\mathbb{E}[\boldsymbol{\nu}_w] = \mathbf{0}$, where $\mathbf{0}$ is a 4×1 zero vector.
- $\mathbb{E}[\boldsymbol{\nu}_w \boldsymbol{\nu}_w^T] = \Sigma$, where Σ is a 4×4 time-invariant covariance matrix.
- $\mathbb{E}[\boldsymbol{\nu}_w \boldsymbol{\nu}_{w-k}^T] = 0$, for any $0 < k < w$. That is, there is no serial correlation across time.

Fig. 8, shows the VAR model, described in Eq. (5), trained on the the first 30 weeks of estimated IRM parameters. The estimated parameters of the IRM are shown in black. The solid lines represents the training data (i.e. the first 30 weeks of IRM parameters), while the dotted lines represents the remaining 8 weeks of IRM parameters. The solid blue lines are the expected behaviour (governed by Eq. (5)) of the fitted VAR. The solid red lines is the average predicted value of 1000 simulations of the fitted VAR model on the remaining 8 weeks of IRM parameters. Lastly, the red dashed lines are 95% confidence envelopes of these simulations, i.e. 95% of the IRM parameters simulated the fitted VAR model were within the two dashed lines.

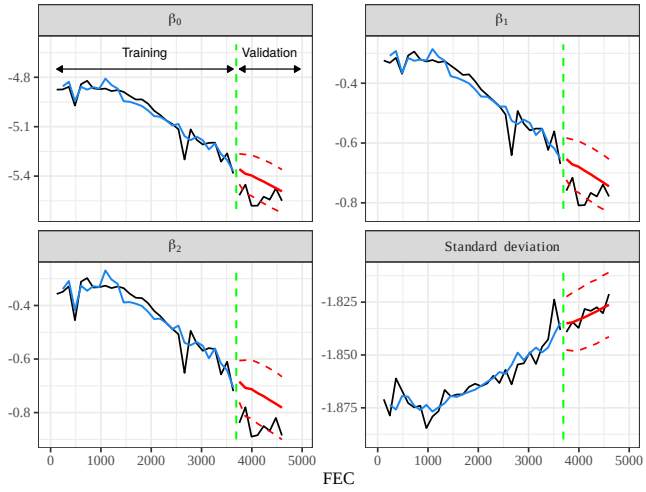

Fig. 8. The parameters of the IRM. The solid black lines correspond to the measured parameters of the IRM for the training and test data (the first 30 weeks and last 8 weeks). The solid blue and red curves correspond to the expected and predicted parameters, under the estimated VAR model, respectively. The red dashed lines are 95% confidence envelopes for the parameter predictions using the estimated VAR.

Comparing the estimated IRM parameters and those predicted under the VAR, for the weeks used to train the VAR, the solid blue lines are sitting almost on top of the solid black lines – indicating a good fit. This is further supported by the root mean square error (RMSE) and mean absolute percentage error (MAPE), which across the four parameters was at most 0.04 and 0.06, respectively. Furthermore, while the the red solid lines are not always directly on top of the dotted lines, the dotted lines are almost always within the 95% confidence envelopes, which gives confidence to the choice of model, and the predictions made by the trained VAR.

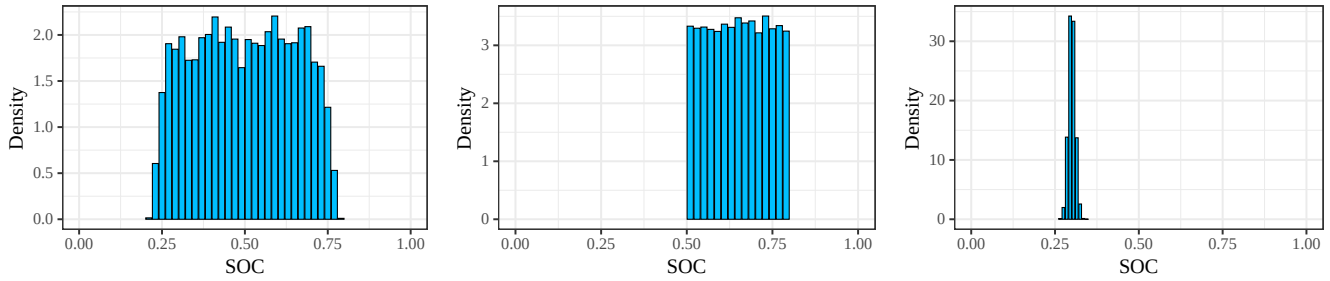

Fig. 9. Histograms for different choices of the marginal SOC distributions. The left, middle, and right panels, shows an SOC distribution learned from the ageing data, a uniform distribution on the interval $[0.5, 0.8]$, and a beta distribution with mean 0.3 and variance 0.0001.

2) Additional SOC information:

The additional SOC information could be as little as a single value, or as much as a distribution over the SOC domain. While providing a distribution may slightly increases the variation in the prediction of the internal resistance, it has one clear advantage: it can be interpreted as the future use of the battery. Furthermore, a distribution over the SOC domain can be learned from the ageing data.

Fig. 9 shows three possible distributions which could used as additional SOC information. The left-most panel is learned from the ageing data, the middle panel is a uniform distribution on the interval $[0.5, 0.8]$, and the right-most panel is a beta distribution with mean 0.3 and variance 0.0001. The behaviour of the learned SOC distribution is mostly concentrated between 25 and 75% SOC, after-which it fades to until it reaches 20 and 80% SOC, respectively.

The histograms represent very different usage behaviours, and will yield different results, when used to predict the internal resistance.

C. Predicting battery resistance degradation

Given a VAR fitted to the parameters of the IRM, and additional the SOC information, then the battery's internal resistance can be predicted to up to some future week W, by the following three steps:

(1) Draw a time-series of the parameters with length W from the fitted VAR.
(2) If a distribution of SOC has been provided, then draw W values from the given distribution. If only a single value was provided pass it along to item (3).
(3) Using the IRM, calculate the expected internal resistance of the IRM using the sampled time-series from item (1), and the provided SOC from item (2).

Repeating this process N times, a posterior predictive distribution can be obtained for the internal resistance up to some future point W.

The posterior distribution of the internal resistance can be used to determine the end-of-life. However, as the posterior distribution is probabilistic, and not deterministic, two limits need to be defined:

(1) End-of-life criterion, L_{EOL}: An upper limit on the internal resistance.
(2) Failure probability, L_F: An upper limit on the probability of seeing a value larger than or equal to L_{EOL}.

Given the limits L_{EOL} and L_F, the end-of-life can be defined as the week W_L where the probability of internal resistance being larger L_{EOL} exceeds L_F.

In the remainder of the paper, L_{EOL} will be set 1.5 times the expected internal resistance of the week 1, and L_F will be set at 1%. Note: that as the expected internal resistance is a function of SOC, it follows that L_{EOL} also becomes function of SOC.

Using the scheme presented above 10000 simulations are made of the internal resistance for a total of 100 weeks, i.e. $N = 10000$ and $W = 100$. In every simulation, the SOC distribution used for the first 38 weeks of ageing was the distribution learned from the ageing data (i.e. the left-most panel of Fig. 9). Fig.'s 10-12 show posterior internal resistance distributions using different SOC distributions for weeks past week 38.

Fig. 10 shows boxplots of the posterior distribution of the internal resistance of every given week. The red line is used to indicate week 38 (the last week of measurements). The points overlaying the boxplots are the internal resistances measured using reference performance test performed at the end of that week. The blue, black, and orange colour corresponds to internal resistance measured at 20, 50, and 80% SOC, respectively. During the first 38 weeks it is clear that the measured internal resistances are well within the posterior distribution of the internal resistance found with the scheme presented in this paper. The boxplots past week 38 are sampled under the assumption that the SOC distribution was the same as during the first 38 weeks of use, i.e. it use the distribution depicted in the left-most panel of Fig. 9. The boxplots past the red line seems to have little increase in the median internal resistance, but the variance increases and, therefore, so does the tendency to see more extreme values.

Fig. 11 and 12 are similar in construction to Fig. 10, but the SOC distribution used after week 38 was the uniform and the beta distributions shown in the middle and right-most panels of Fig. 9. The immediate difference between the figures is the increase in the median internal resistance after week 38. This is a very direct consequence of the selected SOC distribution. The SOC distribution learned from the ageing data, is concentrated between 0.2 and 0.8, thus, it

spends more time around 50% SOC, than the uniform or the beta distribution. As it is known that the internal resistance decreases the closer to 50% the SOC gets (see e.g. Fig.'s 3 and 6), it follows that this will lead to smaller internal resistance values when sampled from the posterior internal resistance distribution. The difference in the variation between Fig. 11 and 12 is a result of the asymmetry of the estimated IRM. The curvature for large SOC tends to be higher than the curvature for small SOC, i.e. $\beta_2 > \beta_1$. The differences in expected internal resistance will lead to differences in the estimated EOL.

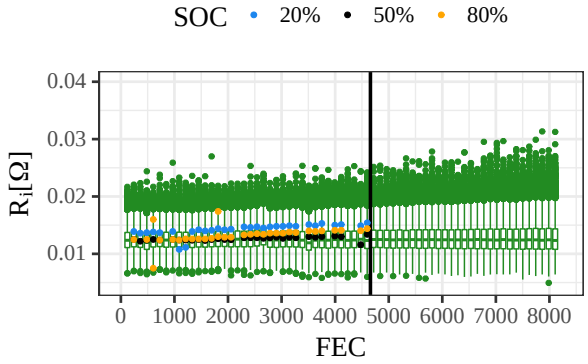

Fig. 10. Boxplots of the predicted resistance model against FEC. The vertical black line corresponds to 38 weeks of operation, and the blue, black, and orange points are the internal resistances measured at 20, 50, and 80%, respectively, using reference performance tests. The posterior distributions of the internal resistance was sampled using the learned SOC distribution seen in the left-most panel of Fig. 9.

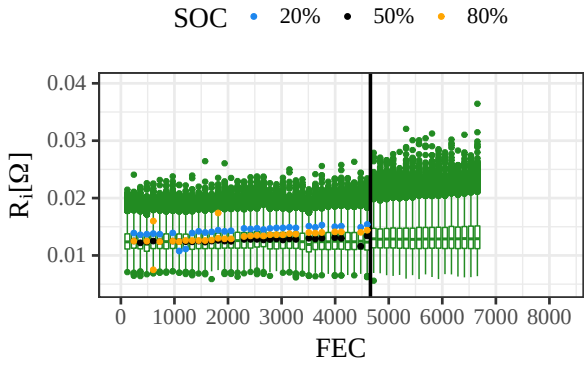

Fig. 11. Boxplots of the predicted resistance model against FEC. The vertical black line corresponds to 38 weeks of operation, and the blue, black, and orange points are the internal resistances measured at 20, 50, and 80%, respectively, using reference performance tests. The posterior distributions of the internal resistance was sampled using the uniform SOC distribution seen in the middle panel of Fig. 9.

The EOL for each of the three usage scenarios was found by calculating empirically the probability of being larger than L_{EOL}, and then determining when this empirical probability was larger than L_F (in this case 1%). A plot of the empirical probability for each week is shown in Fig. 13. The red, green, and blue curves correspond to using the learned, the uniform, and the beta SOC distributions shown in Fig. 9, respectively. The figure shows that during the first 38 weeks the empirical probability is comparable (which should be expected, as the same SOC distribution was used during this period), while curves diverge after this point. When a curve hits the failure probability limit, L_F, shown as the black dashed line, the process is stopped. The EOL for the scenarios using the learned, the uniform, or the beta SOC distributions was estimated to be 66, 55, and 61 weeks, respectively.

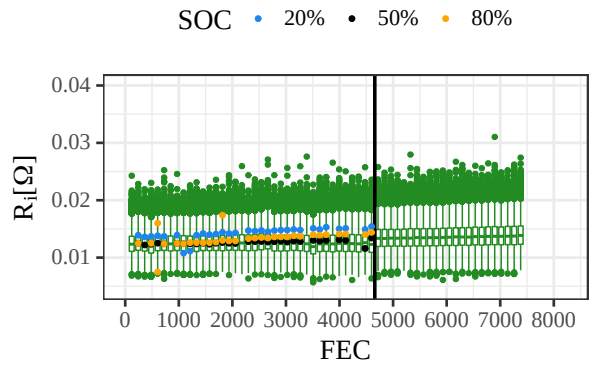

Fig. 12. Boxplots of the predicted resistance model against FEC. The vertical black line corresponds to 38 weeks of operation, and the blue, black, and orange points are the internal resistances measured at 20, 50, and 80%, respectively, using reference performance tests. The posterior distributions of the internal resistance was sampled using the beta SOC distribution seen in the right-most panel of Fig. 9.

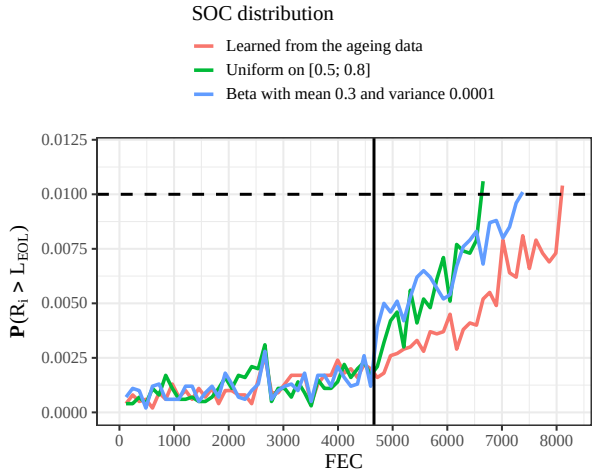

Fig. 13. The probability of observing an internal resistance larger than L_{EOL} (i.e. 1.5 times the expected internal resistance of the first week). The red, green, and blue colours correspond to the scenarios where the SOC distribution used after week 38 (indicated by the solid black line) was the SOC distribution learned from the ageing data, a uniform distribution, and a beta distribution, respectively. The black dashed line is the failure probability, L_F, set at 1%.

V. Battery Lifetime Prediction

Based on the model described in the previous section, the battery internal resistance can be accurately predicted, given

a SOC value and the battery age (i.e., the FEC). However, predicting the battery's lifetime (expressed in the number of FEC) knowing the resistance value and the SOC at which it was determined is also of high interest; to be more precise, the probability distribution of $\mathbb{P}(w|R_i, \text{SOC})$ has to be determined. In order to evaluate this distribution, something has to be assumed about the probability distribution of the SOC, the week, and the joint distribution of resistance, SOC, and week. Starting with the joint distribution, by the definition of conditional probabilities [27] and under the assumption that the SOC and week are independent (which must be true), it can be written:

$$\begin{aligned}\mathbb{P}(\log(R_i), \text{SOC}, W) = \\ \mathbb{P}(\log(R_i)|\text{SOC}, W)\mathbb{P}(\text{SOC})\mathbb{P}(W).\end{aligned} \tag{6}$$

Thus, the joint distribution can be split into three parts, $\mathbb{P}(\log(R_i)|\text{SOC}, W)$, $\mathbb{P}(\text{SOC})$, and $\mathbb{P}(W)$. The conditional distribution of the internal resistance given the SOC and week, $\mathbb{P}(\log(R_i)|\text{SOC}, W)$, is the model described in the previous section. Furthermore, the marginal distributions of the SOC and week, $\mathbb{P}(\text{SOC})$ and $\mathbb{P}(W)$, respectively, have to be defined. In this context, these distributions should be interpreted as a priori information. That is, if any prior information about the distribution of SOC or week are known, they should be considered at this point. The priors on the SOC and the week should be thought of as measurement error and not future usage of the battery (unlike the additional SOC information mentioned in Section IV-B2). In this paper, it will be assumed that any value of SOC and week is equally likely a priori. Consequently, it is assumed that the battery SOC follows a continuous uniform distribution on the unit interval and the week will follow a discrete uniform distribution over the set of possible weeks. Following this reasoning, the posterior distribution of the weeks, given the battery resistance and SOC can be calculated using:

$$\begin{aligned}\mathbb{P}(W|\log(R_i), \text{SOC}) = \\ \frac{\mathbb{P}(\log(R_i)|\text{SOC}, W)\mathbb{P}(\text{SOC})\mathbb{P}(W)}{\sum_{w=1}^{W_L}\mathbb{P}(\log(R_i)|\text{SOC}, w)\mathbb{P}(\text{SOC})\mathbb{P}(w)}\end{aligned} \tag{7}$$

The left-hand side of Eq. (7) is dependent on the battery resistance and SOC. Thus, given a measured resistance at a specified SOC, we have a distribution describing the probability of originating from each of the W_L weeks. If it can be assumed that W_L is the EOL, then this distribution is directly related to the remaining useful life (RUL). In fact the probability of the RUL being exactly r weeks, can be found as:

$$\mathbb{P}\left(r|\log(R_i), \text{SOC}\right) = \mathbb{P}\left(W_{L-r}|\log(R_i), \text{SOC}\right).$$

Fig. 14 shows the distribution of the RUL, given an assumed observed internal resistance of 20 $m\Omega$, and an EOL estimated using the SOC distribution learned from the ageing information (under this assumption the EOL was 66 weeks in accordance with Section IV-C). The three plots assume this internal resistance was measured at 50%, 65%, and 80% SOC shown on the left, in the middle, and on the right-hand panel, respectively. The blue shaded areas are 90% high posterior density regions, it shows that, with 90% certainty, that the age of the battery is within the shaded areas. The figures show that as the SOC increases from 50% to 65% the probability mass functions (the solid black line) gets pushed towards 0 remaining FEC. That is, if an internal resistance of 20 $m\Omega$ is observed at 65% compared of 50% SOC, the battery is expected to be slightly older (or have less remaining FEC). When the SOC is increased to 80%, the RUL probability distribution looks vastly different; its mode is shifted from 0 to around 3000 remaining FEC, and the high posterior density region is moves from $[3505; 0]$ to $[5566; 726]$. That is, if an internal resistance of 20 $m\Omega$ is observed at 80% there is 90% of the remaining FEC being in $[5566; 726]$, and most likely around 3000.

The median (and any other quantile of the posterior distribution) can be found by looking at the cumulative posterior probability function. That is, the cumulative sum of the probability mass function, i.e. the cumulative sum of the black curves in Fig. 14. The median RUL for the three curves shown in Fig. 14 are 1648, 1118, and 3112 FEC, respectively. That is, given an observed internal resistance of 20 $m\Omega$ at each of the specified SOC, there is a 50% probability, that the battery has 1648, 1118, and 3112 (or less) FEC remaining, before the probability has reached EOL (i.e. probability of observing an internal resistance larger than L_{EOL} is more than L_F).

VI. Conclusions

The internal resistance of a Li-ion battery was extracted from a dynamic profile, and a log-linear model associating these values with the SOC was proposed. The parameters of the proposed model were estimated on a week-by-week basis in order to track and model them as a function of time. Given the estimated parameters, the time-varying nature was modelled using a VAR process. It was shown that the VAR could capture the long-term behaviour of the change in the internal resistance (through parameters of the log-linear model). Furthermore, it was shown that by predicting the VAR into the future, it is possible to ascertain posterior distribution of the internal resistance for the predicted VAR period. Setting an EOL criterion to 1.5 times the initial expected internal resistance and a probability failure limit to 1%, the posterior predictive distribution of the internal resistance, can used to find an estimated EOL of the battery. The estimated EOL is heavily dependent on the choice of additional SOC information provided, comparing e.g. using the learned SOC distribution to a simple uniform distribution yielded a difference 11 weeks (the former is estimated to reach EOL in 66 weeks, and the latter 55 weeks). Lastly, using the estimated EOL and VAR model, it was shown that if an

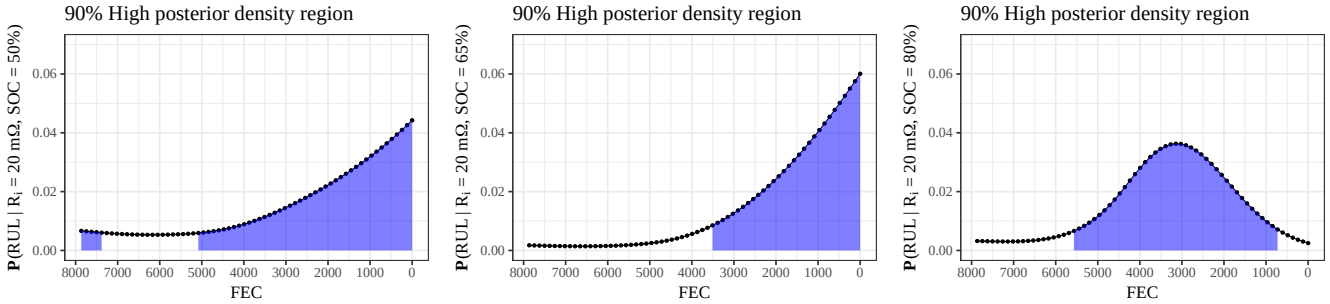

Fig. 14. The posterior probability mass function of the RUL. The blue shaded areas are 90% high posterior density regions. An internal resistance of 20 $m\Omega$ measured at an SOC of 50%, 65%, and 80% for the left-, middle-, and right-hand, respectively.

internal resistance of 20 $m\Omega$ was measured at 65% SOC, then the RUL of a battery was estimated to be at most 3505 FEC with 90% probability, at most 1118 FEC with 50% probability, and at most 161 FEC with 10% probability.

ACKNOWLEDGEMENTS

This work has been part of the "CloudBMS – The New Generation of Intelligent Battery Management Systems" research and development project, project number 64017-05167. The authors gratefully acknowledge EUDP Denmark for providing the financial support necessary for carrying out this work.

REFERENCES

[1] T. Reddy, "Linden's Handbook of Batteries," 4th edition, McGraw Hill, 2010.

[2] Electrically propelled road vehicles – Test specification for lithium-ion traction battery packs and systems – Part 1: High-power applications, ISO 12405-1:2011.

[3] A.-I. Stroe, "Analysis of Performance and Degradation for Lithium Titanate Oxide Batteries," PhD Thesis, Aalborg University, 2018.

[4] D.-I. Stroe, M. Swierczynski, S.K. Kær, E. Martinez-Laserna, and E. Sarasketa-Zabala, "Accelerated Aging of Lithium-Ion Batteries based on Electric Vehicle Mission Profile," 2017 IEEE Energy Conversion Congress and Exposition (ECCE), Cincinnati, OH, pp. 5631-5637, 2017.

[5] N. Nieto et al., "Thermal Modeling of Large Format Lithium-Ion Cells," Journal of The Electrochemical Society, vol. 160, pp. A212-A217, 2013.

[6] D.-I. Stroe, M. Swierczynski, S.K. Kær, R. Teodorescu, "Degradation Behavior of Lithium-Ion batteries during Calendar Ageing – The Case of the Internal Resistance Increase," IEEE Transactions on Industry Applications, vol. 54, pp. 517-525, 2018.

[7] M. Ecker, N. Nieto, S. Kabitz, J. Schmalstieg, H. Blanke, A. Warnecke, D. U. Sauer, "Calendar and cycle life study of Li(NiMnCo)O2-based 18650 lithium-ion batteries," Journal of Power Sources, vol. 248, pp. 839-851, 2014.

[8] H.-G. Schweiger et al., "Comparison of Several Methods for Determining the Internal Resistance of Lithium Ion Cells," Sensors, vol. 10, pp. 5604-5625, 2010.

[9] M.A. Patila, P. Tagadea, K.S. Hariharana, S.M. Kolakea, T. Song, T. Yeo, and S. Doo, "A novel multistage Support Vector Machine based approach for Li ion battery remaining useful life estimation," Applied Energy, vol. 159, pp. 285-297, 2015.

[10] V.T. Trana, H.T. Phama, B.-S. Yanga, and T.T. Nguyen, "Machine performance degradation assessment and remaining useful life prediction using proportional hazard model and support vector machine," Mechanical Systems and Signal Processing, vol. 32, pp. 320-330, 2012.

[11] J. Meng, L. Cai, G. Luo, D.-I. Stroe, and R. Teodorescu, "Lithium-ion battery state of health estimation with short-term current pulse test and support vector machine," Microelectronics Reliability, vol. 88-90, pp. 1216-1220, 2018.

[12] J. Wu, Y. Wang, X. Zhang, and Z. Chen, "A novel state of health estimation method of Li-ion battery using group method of data handling," Power Sources, vol. 327, pp. 457-464, 2016.

[13] P. Guo, Z. Cheng, and L. Yang, "A data-driven remaining capacity estimation approach for lithium-ion batteries based on charging health feature extraction," Power Sources, vol. 412, pp. 442-450, 2019.

[14] D. Yang, Y. Wang, R. Pan, R. Chen, and Z. Chen, "A neural network based state-of-health estimation of lithium-ion battery in electric vehicles," 8th International Conference on Applied Energy, Energy Procedia, vol. 105, pp. 2059-2064, 2017.

[15] A. A. Hussein, "Adaptive Artificial Neural Network-Based Models for Instantaneous Power Estimation Enhancement in Electric Vehicles' Li-Ion Batteries", IEEE Transactions on Industry Applications, vol. 55, pp. 840-849, 2019.

[16] Y. Liu, Z. He, M. Gao, Y. Li, G. Liu, "Dual Estimation of Lithium-ion Battery Internal Resistance and SOC Based on the UKF," 2012 5th International Congress on Image and Signal Processing, Chongqing, pp. 1639-1643, 2012.

[17] Y. Fang, R. Xiong, J. Wang, "Estimation of Lithium-Ion Battery State of Charge for Electric Vehicles Based on Dual Extended Kalman Filter," Energy Procedia vol. 152, pp. 574-579, 2018

[18] Y. Zou, X. Hu, H. Ma, and S.E. Li, "Combined State of Charge and State of Health estimation over lithium-ion battery cell cycle lifespan for electric vehicles," Power Sources, vol. 273, pp. 793-803, 2015.

[19] H. He, R. Xiong, H. Guo, and S. Li, "Comparison study on the battery models used for the energy management of batteries in electric vehicles," Energy Convers. Manag. vol. 64, pp. 113–121, 2012.

[20] S. Schwunk, N. Armbruster, S. Straub, J. Kehl, and M. Vetter, "Particle filter for state of charge and state of health estimation for lithiume-iron phosphate batteries," Power Sources, vol. 239, pp. 705-710, 2013.

[21] L. Zheng, L. Zhang, J. Zhu, G. Wang, and J. Jiang, "Co-estimation of state-of-charge, capacity and resistance for lithium-ion batteries based on a high-fidelity electrochemical model," Applied Energy, vol. 180, pp. 424-434, 2016.

[22] G.K. Prasad, and C.D. Rahn, "Model based identification of aging parameters in lithium ion batteries," Power Sources, vol. 232, pp. 79-85, 2013.

[23] A. Lievre, A. Sari, P. Venet, A. Hijazi, M. Ouattara-Brigaudet, S. Pelissier, "Practical Online Estimation of Lithium-Ion BatteryApparent Series Resistance forMild Hybrid Vehicles," IEEE Transactions on Vehicular Technology, vol. 65, no. 6, pp. 4505-4511, 2016.

[24] M. Mathew, S. Janhunen, M. Rashid, F. Long, and M. Fowler, "Comparative Analysis of Lithium-Ion Battery Resistance Estimation Techniques for Battery Management Systems," Energies, vol. 11, 1490, 2018.

[25] S. B. Vilsen, S. K. Kær, and D.-I. Stroe, "Predicting Lithium-ion Battery Resistance Degradation using a Log-Linear Model," In Proceedings of 2019 IEEE Energy Conversion Congress and Exposition (ECCE), pp. 1136-1143, 2019.

[26] R. H. Shumway and D. S. Stoffer, "Time Series Analysis and Its Applications," 3rd edition, Springer 2010.

[27] P. Olofsson and M. Andersson, "Probability, statistics, and stochastic processes," 2nd edition, Wiley 2012.

[28] D.-I. Stroe, "Lifetime Models for Lithium-ion Batteries used in Virtual Power Plant Applications," PhD Thesis, Aalborg University, 2014.

[29] A.-I. Stroe, V. Knap, and D.-I. Stroe, "Comparison of lithium-ion battery performance at beginning-of-life and end-of-life," Microelectronics Reliability, vol. 88-90, 1251-1255, 2018.